Published in final edited form as:
Mol Nutr Food Res. 2013 October ; 57(10): 1718–1728. doi:10.1002/mnfr.201200794.

Xanthohumol ameliorates atherosclerotic plaque formation, hypercholesterolemia, and hepatic steatosis in *ApoE*-deficient mice

Prakash Doddapattar[1,*], **Branislav Radović**[1,*], **Jay V. Patankar**[1], **Sascha Obrowsky**[1], **Katharina Jandl**[1,2], **Christoph Nusshold**[1], **Dagmar Kolb**[3], **Nemanja Vujić**[1], **Lalit Doshi**[1], **Prakash G. Chandak**[1], **Madeleine Goeritzer**[1], **Helmut Ahammer**[4], **Gerald Hoefler**[5], **Wolfgang Sattler**[1], and **Dagmar Kratky**[1,**]

[1]Institute of Molecular Biology and Biochemistry, Center of Molecular Medicine, Medical University of Graz, Graz, Austria

[2]Institute of Experimental and Clinical Pharmacology, Medical University of Graz, Graz, Austria

[3]Core Facility Ultrastructure Analysis/Institute of Cell Biology, Histology and Embryology, Medical University of Graz, Graz, Austria

[4]Institute of Biophysics, Medical University of Graz, Graz, Austria

[5]Institute of Pathology, Medical University of Graz, Graz, Austria

Abstract

Scope—Xanthohumol (XN), a prenylated antioxidative and anti-inflammatory chalcone from hops, exhibits positive effects on lipid and glucose metabolism. Based on its favorable biological properties, we investigated whether XN attenuates atherosclerosis in western-type diet-fed apolipoprotein-E-deficient (*ApoE*$^{-/-}$) mice.

Methods and results—XN supplementation markedly reduced plasma cholesterol concentrations, decreased atherosclerotic lesion area, and attenuated plasma concentrations of the proinflammatory cytokine monocyte chemoattractant protein 1. Decreased hepatic triglyceride and cholesterol content, activation of AMP-activated protein kinase, phosphorylation and inactivation of acetyl-CoA carboxylase, and reduced expression levels of mature sterol regulatory element-binding protein (SREBP)-2 and SREBP-1c mRNA indicate reduced lipogenesis in the liver of XN-fed *ApoE*$^{-/-}$ mice. Concomitant induction of hepatic mRNA expression of carnitine palmitoyltransferase-1a in *ApoE*$^{-/-}$ mice-administered XN suggests increased fatty acid beta-oxidation. Fecal cholesterol concentrations were also markedly increased in XN-fed *ApoE*$^{-/-}$ mice compared with mice fed western-type diet alone.

Conclusion—The atheroprotective effects of XN might be attributed to combined beneficial effects on plasma cholesterol and monocyte chemoattractant protein 1 concentrations and hepatic lipid metabolism via activation of AMP-activated protein kinase.

Correspondence: Dr. Branislav Radovic, Institute of Molecular Biology and Biochemistry, Medical University of Graz, Harrachgasse 21/3, 8010 Graz, Austria, branislav.radovic@medunigraz.at, **Fax:** +43-316-380-9615. **Additional corresponding author: Professor Dagmar Kratky, dagmar.kratky@medunigraz.at.
*These authors contributed equally to this work.

Additional supporting information may be found in the online version of this article at the publisher's web-site

The authors have declared no conflict of interest.

Europe PMC Funders Author Manuscripts

Keywords

AMPK signaling; Atherosclerosis; Inflammation; Lipid metabolism; Xanthohumol

1 Introduction

Animal experiments and clinical investigations have established that high circulating concentrations of cholesterol promote cardiovascular disease [1]. Although hypercholesterolemia is associated with cardiovascular complications in approximately 50% of all patients, inflammatory mechanisms are pathologically important in atherosclerosis [2, 3], which is characterized by slowly progressing plaque formation in the vessel wall of large and medium arteries.

Plasma cholesterol levels reflect the balance between two processes responsible for maintaining cholesterol homeostasis: intestinal absorption and reverse cholesterol transport. The intestine plays an important role by serving as the site of both absorption of dietary cholesterol and re-absorption of biliary cholesterol. Reverse cholesterol transport is a pathway by which cholesterol from peripheral tissues is transported to the liver for biliary excretion [4]. The liver regulates synthesis, secretion, and clearance of cholesterol-rich lipoproteins, and determines the amount of peripheral cholesterol excreted into the bile, either as free cholesterol (FC) or after conversion into bile acids [5,6].

Xanthohumol (XN) (Supporting Information Fig. S1) is a prenylated flavonoid found in hops, inflorescences of the female hop plant (*Humulus lupulus* L.). XN exerts antioxidative, chemopreventive, and anti-inflammatory effects. Using HepG2 cells as a model system, Casaschi et al. showed inhibition of triglyceride (TG) and apolipoprotein (Apo)B secretion associated with increased cellular ApoB degradation and lower activity of microsomal TG transfer protein by XN treatment [7]. XN-fed genetically obese KK-A^y mice exhibited lowered plasma glucose, plasma and hepatic TG concentrations, and adipose tissue weight as well as increased plasma adiponectin levels. In addition, mRNA expression of hepatic genes involved in fatty acid synthesis and gluconeogenesis was decreased [8]. In 3T3-L1 adipocytes, Yang et al. reported reduced lipid content and decreased adipocyte marker proteins after incubation with XN [9]. XN also lowers body weight and fasting plasma glucose in obese male Zucker fa/fa rats [10]. Decreased production of the proinflammatory cytokines IL-1 beta, inducible nitric oxide synthase [11], and IL-12 [12] in LPS-activated macrophages, and reduced monocyte chemoattractant protein 1 (MCP-1) and tumor necrosis factor alpha concentrations were observed after XN treatment in mouse macrophages and human monocytes [13]. These beneficial effects of XN on inflammation, obesity, and hyperlipidemia as important risk factors for cardiovascular disease prompted us to study the effects of XN on atherosclerosis development in ApoE-deficient (*ApoE*$^{-/-}$; where ApoE is apoliprotein E) mice, which develop severe hypercholesterolemia and atherosclerosis in the aorta and coronary arteries [14].

In this study, we demonstrate that addition of XN to western-type diet (WTD) ameliorates atherosclerotic plaque formation in *ApoE*$^{-/-}$ mice by positively affecting plasma cholesterol and MCP-1 concentrations and hepatic lipid metabolism via activation of AMP-activated protein kinase (AMPK).

Europe PMC Funders Author Manuscripts

2 Materials and methods

2.1 Animals

Female *ApoE*$^{-/-}$ mice (The Jackson Laboratory, Bar Harbor, ME, USA), maintained on a regular 12 h dark/light cycle, were fed chow diet containing 4.3% fat and 21% protein (Ssniff, Soest, Germany). At the age of 8–9 weeks, they were divided into two groups (n = 8–9) designed to have similar mean fasted plasma cholesterol concentrations and challenged with WTD (21% fat, 0.2% cholesterol; Ssniff) or WTD + XN (300 mg/kg body weight/day) for 8 weeks to induce atherosclerotic plaque formation.

XN (Xantho-flav) was obtained from Hopsteiner®, Mainburg, Germany. For extraction (http://www.lfl.bayern.de/ipz/hopfen/10585/wk07_bericht_2.pdf), whole hops were mixed with 90% ethanol to obtain the raw extract containing hop acids and polar components such as polyphenols. Prenylflavonoids were re-extracted from pure resin extract with CO_2. A selective separation of prenylflavonoids from the extraction residue consisting of CO_2 nonsoluble resins and prenylflavonoids with 5–20% xanthohumol was performed with polyvinylpyrrolidone. An ethanolic solution of “Xantho-Extract” passed polyvinylpyrrolidone; the prenylflavonoids were adsorbed and then eluted by ethylacetate. Gentle evaporation of the solvent under vacuum resulted in a yellow powder (Xantho-Flav) which only consists of prenylflavonoids with xanthohumol as main ingredient (80% in our substance). The purity of XN was determined by the manufacturer using HPLC by UV detection at 370 nm using pure XN as a calibrator.

XN was mixed with WTD powder, lyophilized, and administered as pellets to mice ad libitum. Blood was collected after 4 and 8 weeks of feeding. Animals were sacrificed and organs collected. One additional cohort (n = 5) was fed WTD ± XN for 4 weeks to determine fractional cholesterol absorption. In addition, plasma isolated from these mice was used for estimation of lipid parameters and added to the values obtained in the first cohort after 4 weeks of feeding. This explains the inconsistence in the number of mice used in different experiments.

LDL receptor (*Ldlr*)$^{-/-}$ mice (n = 4) (The Jackson Laboratory) were fed WTD or WTD + XN (300 mg/kg body weight/day) for 4 weeks. Thereafter, blood was collected and plasma was isolated for lipid analysis.

All experimental protocols were approved by the Austrian Federal Ministry of Science and Research, Division of Genetic Engineering and Animal Experiments (Vienna, Austria) (BMWF-66.010/0057-II/3b/2011, BMWF-66.010/0159-II/3b/2012).

2.2 Lipid analyses in plasma, liver, small intestine, and feces

Blood was collected from the retro-orbital plexus after overnight fasting and plasma was prepared within 20 min. Plasma TG, FC (DiaSys, Holzheim, Germany), and total cholesterol (TC) (Greiner Diagnostics AG, Bahlingen, Germany) levels were measured spectrophotometrically. Cholesteryl esters (CE) concentrations were calculated as CE = TC − FC. Lipoprotein profiles were determined by fractionation of 200 μL pooled plasma by fast protein LC (FPLC) on a Pharmacia FPLC system (Pfizer Pharma, Karlsruhe, Germany) using a Superose 6 column (Amersham Biosciences, Piscataway, NJ, USA). The lipoproteins were eluted with 10 mM Tris-HCl, 1 mM EDTA, 0.9% NaCl, and 0.02% NaN_3 (pH 7.4). TC and FC concentrations in 0.5 mL fractions were determined using above-mentioned kits. To enhance sensitivity, sodium 3,5-dichloro-2-hydroxy-benzenesulfonate was added to the reaction buffer.

Feces were collected for three consecutive days and dried overnight. During this time, food intake was monitored. Lipids from feces, liver, and the middle part of the small intestine (jejunum) were extracted using 2 mL hexane:isopropanol (3:2, v:v) for 1 h at 4°C. Extracts were dried under a stream of nitrogen. One hundred microliters of 1% Triton X-100 in chloroform was added and dried under nitrogen. Samples were dissolved in 100 μL distilled water for 15 min at 37°C, and TC concentrations were estimated using above-mentioned kits. The readings were normalized to liver (wet) and feces (dry) weight.

2.3 Determination of XN in vivo concentrations

XN was extracted from pooled samples ($n = 4$; fed state) of liver (200 μg protein) and feces (100 mg dry weight) with 300 μL methanol. From plasma (60 μL), XN was extracted with 100 μL methanol. After vortexing for 60 s, samples were centrifuged at 14 000 rpm for 10 min. Supernatants of liver and feces samples were dried under a stream of nitrogen and re-dissolved in 100 μL methanol. Supernatants of plasma samples were used directly after precipitation of plasma proteins. Ten microliters of extracts or standards were separated by RP-HPLC (Waters HPLC 2690 Seperations Module) at a flow rate of 0.7 mL using a Chromasil C_{18} RP column (150 × 4.6 mm, 5 μm particle size; Altmann Analytik, Munich, Germany). The mobile phase consisted of solvent A (ACN, 0.1% formic acid) and solvent B (20% ACN in water, 0.1% formic acid). Analytes were eluted using a gradient ranging from 40:60 A:B (0−4 min), 50:50 A:B (linear, 4−10 min), 0:100 A:B (linear 10−15 min; hold 15−20 min), and 40:60 A:B (20−23 min, linear; 23−28 min hold). A Waters 2487 absorbance detector set to 370 nm was used for detection. XN (eluting at 15.3 min) concentrations were calculated by peak area comparison with external standards.

2.4 Preparation of histological sections and lesion analyses

Atherosclerotic lesions in *ApoE*$^{-/-}$ mice were measured in the aorta and aortic roots after 8 weeks of WTD and WTD + XN feeding. Mice were euthanized and the arterial tree was perfused in situ with PBS (100 mm Hg) for 10 min and 4% neutral-buffered formalin (Carl Roth GmbH, Vienna, Austria) for 15 min via a cannula in the left ventricular apex. After fixing hearts in 4% neutral-buffered formalin, serial sections (8 μm) were cut (HM 560 Cryo-Star; Microm International GmbH, Walldorf, Germany). Images of the atherosclerotic lesion areas in oil red O (Sigma-Aldrich, St. Louis, MO, USA) stained sections were taken with ScanScope T3 whole slide scanner (Aperio Technologies, Bristol, UK). Plaque areas were quantitated by the image processing application software IQM (developed by H. Ahammer). Mean lesion area was calculated from five consecutive oil red O-stained sections, starting at the appearance of the tricuspid valves.

For en face analysis, aortas were dissected, fixed with 4% formalin (in PBS), and plaques were stained with oil red O. Stock solution (0.4% oil red O in 100% isopropanol) was diluted to 60% isopropanol to prepare a fresh working solution. Aortas were rinsed with 60% isopropanol and incubated for 15 min in oil red O working solution. Thereafter they were rinsed again with 60% isopropanol, fixed with pins, and images were taken with an SZX10 microscope (Olympus Austria GmbH, Vienna, Austria) equipped with a DP12 Camera. Images were analyzed using ImageJ software (ImageJ 1.43U, NIH, USA).

2.5 Histochemistry

For conventional light microscopy, livers of mice fed WTD or WTD + XN were fixed in 4% neutral-buffered formalin solution for 24 h and embedded in paraffin. Five micrometers sections were deparaffinized and subjected to hematoxylin/eosin staining. Sections were rinsed with distilled water and nuclei were stained with hematoxylin (0.7%) for 4 min. After rinsing with water, sections were differentiated with 0.3% acid alcohol, rinsed with water, and stained for 2 min with 1% eosin. Slides were dried and mounted for microscopy. For

histochemical staining with oil red O, 7 μm cryosections were fixed with 10% formaldehyde. Five min after the fixation, sections were stained with fresh oil red O working solution (see above) for 10 min to detect lipid accumulation. After rinsing with distilled water, the slides were stained with hematoxylin for 5 min, washed with distilled water for 15 min, and mounted. Images of oil red O-stained liver sections were taken with a Nikon Eclipse 80i microscope (Nikon, Vienna, Austria).

2.6 Real-time PCR analyses

Total RNA from aorta, liver, and small intestine was isolated using TriFast (Peqlab, Erlangen, Germany) according to the manufacturer's protocol. Two micrograms RNA were reverse transcribed using the High Capacity cDNA Reverse Transcription Kit (Applied Biosystems, Foster City, CA, USA). Real-time PCR was performed on a LightCycler 480 system (Roche, Basel, Switzerland) using the Quantifast SYBR Green PCR kit (Qiagen, Hilden, Germany). Relative expression of genes was normalized to the expression of cyclophilin A as internal reference. Calculations of data were performed using the ddCt method. Following primer sequences were used:

Abcb4_f: AGGCAGCGAGGAAACGGAA

Abcb4_r: TGCTGATGCTGCCTAGTTCAA

Abcg1_f: GGAGTTGCTAAGGACCTTCTTG

Abcg1_r: GACGCTGACTATAAGAGAGACC

Abcg5_f: AGAGGGCCTCACATCAACAGA

Abcg5_r: CTGACGCTGTAGGACACATGC

Abcg8_f: AGTGGTCAGTCCAACACTCTG

Abcg8_r: GAGACCTCCAGGGTATCTTGAA

Cpt-1a_f: CTCCGCCTGAGCCATGAAG

Cpt-1a_r: CACCAGTGATGATGCCATTCT

Scd1_f: CCGGAGACCCCTTAGATCGA

Scd1_r: TAGCCTGTAAAAGATTTCTGCAAACC

Srebp-1c_f: ATCGGCGCGGAAGCTGTCGGGGTAGCGTC

Srebp-1c_r: ACTGTCTTGGTTGTTGATGAGCTGGAGCAT

Srb1_f: GAGCACGTTCTACACGCAG

Srb1_r: GGTCTGACCAAGCTATCAGGTT

2.7 Separation of fat cake by ultracentrifugation

To separate lipids from water soluble components, 100 μL liver lysates were centrifuged at 100 000 × *g* for 60 min at 4°C. Thereafter images of the ultracentrifuge tubes showing fat cakes on top of liquid fractions were captured.

2.8 Western blotting

Forty micrograms of sonicated liver protein lysates were separated by 10% SDS-PAGE and blotted onto nitrocellulose Protran BA85 membranes (Whatman, Vienna, Austria). Membranes were blocked with 5% nonfat milk for 2 h and incubated with rabbit polyclonal antibodies against ATP-binding cassette transporter (ABC) G1 (1:500) (Novus Biologicals, Littleton, CO, USA), ACCα (1:1000) (where ACC is acetyl-CoA carboxylase),

phosphorylated (p)ACCα(Ser79) (1:1000), pAMPK (Ser172) (1:1000), and SREBP-2 (1:1000; where SREBP is sterol regulatory element-binding protein), (Cell Signaling Technology, Danvers, MA, USA), pHMGCR(Ser872) (HMGCR, 3-hydroxy-3-methylglutaryl CoA reductase) (Biorbyt, Cambridge, UK), and a monoclonal antimouse β-actin antibody (1:5000) (Sigma-Aldrich). Specifically bound Igs were detected in a second reaction using horseradish peroxidase-conjugated IgG goat antirabbit (1:5000) (Santa Cruz Biotechnology) and rabbit antimouse (1:2000) (Dako, Glostrup, Denmark) antibodies and visualized by enhanced chemiluminescence substrate (ECL Plus; GE Healthcare, Piscataway, NJ, USA) on an AGFA Curix Ultra X-ray film and Biorad ChemiDoc™ MP Imaging System (BioRad Laboratories Inc, Hercules, CA, USA).

2.9 ELISA

Serum was collected from overnight fasted WTD and WTD + XN fed *ApoE*$^{-/-}$ mice. Serum MCP-1 and IL-6 levels were measured by ELISA (R&D Systems Inc., Minneapolis, MN, USA) according to the manufacturer's protocol.

2.10 Transmission electron microscopy

Liver tissue was dissected using a Zeiss OPI1 surgical microscope (Carl Zeiss, Oberkochen, Germany). Small tissue fragments were fixed in 2.5% (wt/v) glutaraldehyde and 2% (wt/v) paraformaldehyde in 0.1 M phosphate buffer (pH 7.4) for 2 h, postfixed in 2% (wt/v) osmium tetroxide for 2 h at room temperature, dehydrated in graded series of ethanol, and embedded in a TAAB epoxy resin. Sections (70-nm thick) were contrasted with uranyl acetate and lead citrate. Images were taken using an FEI Tecnai G^2 20 transmission electron microscope (FEI Eindhoven, Eindhoven, the Netherlands) with a Gatan ultrascan 1000 CCD camera. Acceleration voltage used was 120 kV.

2.11 Fractional cholesterol absorption

Fractional cholesterol absorption was measured by using the fecal dual-isotope ratio method as described previously [15]. Briefly, *ApoE*$^{-/-}$ mice ($n = 5$) fed 4 weeks WTD diet with or without XN were fasted for 4 h before they were given a single intragastric dose of 100 μL corn oil containing 0.2 μCi ^{3}H-sitostanol (ARC Inc., St. Louis, MO, USA) and 0.1 μCi ^{14}C-cholesterol (ARC Inc.). Feces were collected for 48 h. Fecal lipids were isolated by Folch extraction, and radioactivity was determined by liquid scintillation counting. Fractional cholesterol absorption was calculated as

$$\%\text{absorption} = \left(\left(\text{dose}\left[14\text{C}\right]:\left[^3\text{H}\right] - \text{fecal}\left[^{14}\text{C}\right]:\left[^3\text{H}\right]\right)/\text{dose}\left[^{14}\text{C}\right]:\left[^3\text{H}\right]\right)\times 100 \quad (1)$$

2.12 Statistics

Statistical analyses (except for real-time PCR) were performed with the GraphPad Prism 5.0 software. Significances were determined by Student's *t*-test. Data are presented as mean values ± SEM. $p < 0.05$ (*), $p \leq 0.01$ (**), and $p \leq 0.001$ (***).

3 Results

3.1 Reduced plaque formation in XN-fed ApoE$^{-/-}$ mice

To elucidate the effect of XN treatment on atherosclerotic plaque formation, we fed *ApoE*$^{-/-}$ mice WTD ± XN for 8 weeks. This feeding regimen resulted in 61 nmol/L circulating XN in the plasma of fed animals. In overnight fasted mice XN was not detectable (Table 1). First, we examined oil red O-stained lesions in aortic valve sections and en face aortas. Mice-administered XN exhibited decreased plaque formation (Fig. 1) as shown by 43% reduction

in total lesion area of thoracic aorta (Fig. 1A) and 33% reduction in mean lesion area of transverse heart sections in the vicinity of the aortic root (Fig. 1B)

3.2 Reduced MCP-1 concentrations in XN-fed ApoE$^{-/-}$ mice

To clarify potential anti-inflammatory effects of XN feeding, we determined serum IL-6 and MCP-1 levels in *ApoE*$^{-/-}$ mice fed WTD ± XN. These analyses revealed that MCP-1 concentrations were reduced by 43%, whereas dietary XN supplementation was without effects on IL-6 levels (Fig. 2).

3.3 Reduced lipid concentrations in plasma and liver of XN-fed ApoE$^{-/-}$ mice

Increased plasma lipid levels substantially induce initiation and progression of atherosclerosis [1]. We therefore measured plasma lipid parameters of overnight fasted mice after 4 and 8 weeks of feeding WTD ± XN, respectively. We found markedly decreased TC (32%), FC (27%), and CE (33%) concentrations after 4 weeks of feeding WTD + XN (Table 1). After 8 weeks, plasma TC, FC, and CE concentrations were significantly reduced in XN-fed *ApoE*$^{-/-}$ mice by 24, 22, and 24%, respectively. Plasma TG levels were comparable between both groups. Lipoprotein profiling revealed that TC and FC concentrations were markedly decreased in the VLDL fraction with no changes in LDL and HDL fractions (Fig. 3).

Next we wanted to elucidate whether XN positively affects plasma cholesterol levels in another mouse model of atherosclerosis. We therefore fed LDL receptor (*Ldlr*)$^{-/-}$ mice WTD ± XN for 4 weeks. Reduced plasma cholesterol concentrations in XN-treated *Ldlr*$^{-/-}$ mice (Supporting Information Table S1 and Fig. S2) indicate that XN regulates plasma cholesterol concentrations during WTD feeding independent on ApoE deficiency.

Fluctuations in circulating lipids mainly reflect activities of liver and intestine during lipid absorption, de novo biosynthesis and/or recycling. We observed no difference in fractional cholesterol absorption in response to XN feeding as determined by the fecal dual-isotope ratio method (Supporting Information Fig. S3A). In addition, intestinal cholesterol and TG concentrations were comparable between XN-treated and control *ApoE*$^{-/-}$ mice (Supporting Information Fig. S3B). These data suggest that the effect of XN on plasma lipid levels is not mediated by the small intestine. In contrast, liver lipids (especially cholesterol) were markedly reduced in mice-administered XN. We found decreased hepatic TC (39%), FC (36%), CE (56%), and TG (27%) concentrations (Table 2). Oil red O staining confirmed reduced neutral lipid content in *ApoE*$^{-/-}$ mice fed XN (Fig. 4A). After centrifugation of liver lysates from WTD-fed *ApoE*$^{-/-}$ mice, we observed thick fat cakes, which were absent in XN-fed mice (Fig. 4B). Additionally, electron microscopy revealed smaller lipid droplets in hepatocytes from XN-fed *ApoE*$^{-/-}$ mice (Fig. 4C). No pathological changes were observed in livers of *ApoE*$^{-/-}$ mice fed WTD ± XN according to hematoxylin/eosin staining (Fig. 4D). We further measured XN concentrations in liver and feces to assess relative intestinal absorption of XN. An XN concentration of 24 μg/g liver protein compared with 748 μg/g feces indicated poor intestinal absorption. In agreement with plasma concentrations (Table 1), these data imply that XN is effective at low doses.

3.4 XN reduces hepatic de novo lipogenesis by AMPK activation

To address the question whether the lipid-lowering effect of XN is due to increased excretion into the bile or reduced hepatic biosynthesis, we investigated proteins involved in fatty acid and cholesterol homeostasis. Hepatic mRNA expression levels of SREBP-1c and stearoyl CoA desaturase 1 were reduced in XN-treated *ApoE*$^{-/-}$ mice (Fig. 5A). Phosphorylation of ACC, the key enzyme in de novo fatty acid biosynthesis [16] was significantly induced upon XN treatment (Fig. 5B). To investigate the underlying

mechanism, we next determined AMPK phosphorylation, which was substantially induced in XN-treated *ApoE*$^{-/-}$ livers but almost absent in control *ApoE*$^{-/-}$ mice. Phosphorylated (p)AMPK is known to phosphorylate and inactivate ACC, thereby leading to inhibition of fatty acid [17,18], cholesterol, and TG biosynthesis [19,20]. We hypothesized that lower plasma cholesterol concentrations reflect its decreased supply from the liver as a central organ in de novo cholesterol biosynthesis. We therefore measured the phosphorylated and inactive form of HMGCR and SREBP-2, key proteins in cholesterol biosynthesis. We failed to observe changes in protein expression of pHMGCR, whereas mature SREBP-2 was slightly but significantly downregulated (Fig. 5B). To investigate transcriptional regulation of carnitine palmitoyltransferase (CPT)-1a, the protein responsible for fatty acid import into the mitochondria, we performed real-time PCR analysis. As shown in Fig. 5C mRNA expression of CPT-1a was significantly higher in XN-fed animals indicating the possibility of enhanced fatty acid beta-oxidation.

Finally, we analyzed expression levels of cholesterol transporters and found a moderate but significant increase in the protein abundance of hepatic ABCG1 in XN-treated *ApoE*$^{-/-}$ mice (Fig. 6A). However, ABCA1 and ABCG5/G8 protein expression (data not shown) as well as mRNA levels of ABCG1, ABCG5/G8, ABCB4, and SRB1 (Supporting Information Fig. S4) were comparable between both groups. In agreement with our assumption that XN induces cholesterol excretion from the liver, we found elevated concentrations of TC (40%) in feces of XN-fed *ApoE*$^{-/-}$ mice compared with control mice fed WTD for 8 weeks (Fig. 6B). Food intake, which was monitored during feces collection over 3 days, was comparable in both groups (data not shown).

4 Discussion

This study demonstrates beneficial effects of the prenylflavonoid XN on atherosclerotic plaque formation and hypercholesterolemia in WTD-fed *ApoE*$^{-/-}$ mice. The present data provide evidence that decreased atherosclerosis is a result of combined positive effects on circulating cholesterol and MCP-1 concentrations. Our results also suggest that XN is a potent natural hepatic AMPK activator.

The observed effects are attributed to XN (80% purity) although there is a possibility that other prenylflavonoids contribute as well. The strongest candidates are isoxanthohumol (IXN) and 8-prenylnaringenin (8-PN). Nevertheless, taking a compound of a higher purity would still not eliminate the possibility that these XN metabolites are involved. XN, converted to IXN spontaneously or by gut bacteria, can be further metabolized either by gut bacteria or by cytochrome enzymes in the liver into 8-PN [21, 22]. Twenty-four hours after oral administration of pure XN to rats, concentrations of IXN and 8-PN in the blood reached approximately 50 and 25% of XN concentration, respectively [21]. According to another similar study, IXN concentration was even higher in the blood after 1 h compared with XN, whereas 8-PN was not detected [22]. Additional in vivo experiments using IXN and 8-PN are therefore needed to shed more light on this controversial issue.

After feeding *ApoE*$^{-/-}$ mice with XN-supplemented WTD, we observed markedly reduced circulating cholesterol and MCP-1 concentrations, which are important determinants of atherosclerotic lesion formation [2,23,24]. Recent data showing decreased cholesterol concentrations in atherosclerotic plaques of XN-treated mice expressing human CE transfer protein [25] support our findings. XN has been considered an anti-inflammatory substance according to findings in various in vitro and in vivo studies [11-13, 26-28]. We observed decreased MCP-1 but not significantly reduced IL-6 serum concentrations. In accordance with our results, MCP-1 was the only inflammatory marker found to be increased at the early stage of high fat diet-induced kidney disease, which is characterized by inhibition of

AMPK activity [29]. In addition, it was reported that AMPK activation in vitro and in vivo reduces MCP-1 in urine and kidney [29], adipocytes [30], macrophages [31], and endothelial cells [32]. Additional studies are needed to find the possible link between AMPK activation by XN and the reduction of MCP-1 in serum of *ApoE*$^{-/-}$ mice.

The synthetic polyphenol S17834, which was shown to activate AMPK, inhibits SREBP-1 activity, thereby positively affecting dyslipidemia, liver steatosis, and atherosclerosis in diet-induced insulin-resistant mice [33]. AMPK plays a major role in the control of hepatic metabolism. AMPK phosphorylates multiple targets in the liver in order to acutely switch on alternative catabolic pathways and switch off anabolic pathways. ACC is an important rate-controlling enzyme for the synthesis of malonyl-CoA, which is a critical precursor of fatty acid and TG biosynthesis [16, 34] and an inhibitor of fatty acid beta-oxidation [35]. Thus, phosphorylation and inhibition of ACC by AMPK results in reduced malonyl-CoA concentrations followed by decreased fatty acid biosynthesis and increased mitochondrial fatty acid beta-oxidation via regulation of CPT-1 activity [35]. XN treatment induced the protein expression of the inactive, phosphorylated form of ACC in *ApoE*$^{-/-}$ mice. Consequently, TG concentrations were decreased in XN-treated *ApoE*$^{-/-}$ livers.

Despite its ineffective intestinal uptake, XN bioavailability studies [21, 22, 36] report micromolar concentrations of XN in livers and plasma after oral application. The dose of XN used in this study was not expected to have any adverse effects since it was only one-third of the published safety margin in mice [37-39]. In accordance, no signs of liver toxicity were observed as shown by hematoxylin/eosin staining. XN absorption in the intestine was very low according to the content in feces and compared with plasma and liver concentrations. For potential applications in clinical studies, we are currently improving the feeding method as suggested by Legette et al. [21] to reduce XN doses. Here, we show that XN exerts its activities in the liver by significantly decreasing hepatic lipid levels at concentrations of only 24 μg/g protein. In agreement with reduced de novo lipogenesis, increased CPT-1a mRNA expression in livers of *ApoE*$^{-/-}$ mice-administered XN imply a higher rate of mitochondrial fatty acid beta-oxidation. Although hepatic cholesterol concentrations were reduced (in agreement with reduced protein expression of mature SREBP-2), pHMGCR was unaffected by XN treatment. This phenomenon is difficult to explain since AMPK was also shown to phosphorylate HMGCR thereby resulting in decreased cholesterol biosynthesis [20,33,40,41]. AMPK is important but not the solely metabolic regulator of HMGCR. A natural negative regulator of HMGCR activity is cholesterol itself [40]. Decreased hepatic cholesterol concentration as observed in this study might mask the inhibitory effect of XN on HMGCR via AMPK. Future studies focused on early effects of XN in the liver are needed to proof this assumption.

Activated AMPK also inhibits glycogen synthesis, consecutively increasing glycolysis and glucose transport. AMPK regulates insulin synthesis and secretion as well as modulation of hypothalamic functions involved in the regulation of satiety [42]. This might explain findings by others [8,10] showing beneficial effects of XN on obesity, probably by inducing catabolic AMPK-regulated pathways. The mechanism might be the activation of AMPK by inhibition of the Akt pathway. In fact, several publications have so far reported that XN inhibits the Akt pathway [39, 43-46]. Blocking of Akt increases the AMP/ATP ratio and subsequently activates AMPK [47] since the main cause of AMPK phosphorylation is due to a rise in AMP levels when the energy status of the cell is low.

Plasma cholesterol levels reflect the degree of systemic absorption, usage, de novo production, and recycling. Liver and intestine play crucial roles in the regulation of cholesterol homeostasis. Our data indicate that the small intestine is not involved in cholesterol-lowering effects of XN, since we did not find differences in fractional

cholesterol absorption. These data suggest that increased cholesterol concentrations in feces of *ApoE*$^{-/-}$ mice fed XN result from increased secretion from the liver into the bile. Nozawa [8] reported a sevenfold increased mRNA expression of Cyp7a1, the key enzyme in neutral bile acid biosynthesis, in the liver of KK-A^{y} mice-administered XN. Cyp7a1 mRNA expression, however, was unaffected (data not shown) by XN treatment. Nevertheless, we observed increased cholesterol concentrations in the feces, which might be the result of elevated ABCG1 protein expression. ABCG1 was identified as an important regulator of liver lipid homeostasis. Although the expression levels of ABCG1 in hepatocytes are much lower compared to Kupffer cells, high cholesterol diet feeding might lead to specific stimulation of ABCG1 in parenchymal cells [48]. Disruption of ABCG1 in mice induced massive accumulation of both neutral lipids and phospholipids in hepatocytes, whereas overexpression of human ABCG1 protected liver from dietary fat-induced lipid accumulation [49]. Though it might be expected that liver ABCG1 plays a role in efflux of cellular cholesterol to HDL rather than sterol excretion into bile, it was reported by Ji et al. [50] that ABCG1-deficient primary hepatocytes have a similar capacity to efflux cholesterol to ApoA-I and to form nascent HDL particles compared with control cells. This question is, however, less relevant for our study because we used *ApoE*$^{-/-}$ mice, which are depleted of HDL. Further investigations are needed to clarify whether hepatocytes or Kupffer cells are responsible for increased cholesterol excretion observed in XN-treated *ApoE*$^{-/-}$ mice and to look more closely at the role of ABCG1.

Figure 7 summarizes the data obtained in our study. We conclude that XN ameliorates atherosclerotic plaque formation by improving liver and circulating cholesterol and MCP-1 concentrations. Importantly, we discovered a potent natural agent able to activate AMPK which is, although unspecifically regulated, an emerging target for the treatment of type 2 diabetes, obesity, dyslipidemia, and atherosclerosis.

Supplementary Material

Refer to Web version on PubMed Central for supplementary material.

Acknowledgments

The authors like to thank A. Ibovnik, S. Povoden, and M. Absenger for excellent technical assistance and I. Hindler for mice care. We also thank Dr. Martin Biendl for providing us XN. P.D. is a fellow of the PhD Program Molecular Medicine of the Medical University of Graz. This work was supported by the Grants F30 SFB LIPOTOX, W1226 DK-MCD, P19186, and P22832, which are all funded by the Austrian Science Fund (FWF).

Abbreviations

ABC	ATP-binding cassette transporter
ACC	acetyl-CoA carboxylase
AMPK	AMP-activated protein kinase
ApoE	apoliprotein E
CE	cholesteryl esters
CPT	carnitine palmitoyltransferase
FC	free cholesterol
FPLC	fast protein liquid chromatography
HMGCR	3-hydroxy-3-methylglutaryl CoA reductase

MCP-1	monocyte chemoattractant protein 1
SREBP	sterol regulatory element-binding protein
TC	total cholesterol
TGs	triglycerides
WTD	western-type diet
XN	xanthohumol

References

[1]. Brown MS, Goldstein JL. How LDL receptors influence cholesterol and atherosclerosis. Sci. Am. 1984; 251:58–66. [PubMed: 6390676]

[2]. Hansson GK, Hermansson A. The immune system in atherosclerosis. Nat. Immunol. 2011; 12:204–212. [PubMed: 21321594]

[3]. Ross R. Atherosclerosis—an inflammatory disease. N. Engl. J. Med. 1999; 340:115–126. [PubMed: 9887164]

[4]. Bakkeren HF, Kuipers F, Vonk RJ, Van Berkel TJ. Evidence for reverse cholesterol transport in vivo from liver endothelial cells to parenchymal cells and bile by high-density lipoprotein. Biochem. J. 1990; 268:685–691. [PubMed: 2363705]

[5]. Nestel PJ, Whyte HM, Goodman DS. Distribution and turnover of cholesterol in humans. J. Clin. Invest. 1969; 48:982–991. [PubMed: 5771198]

[6]. Percy-Robb IW, Boyd GS. The synthesis of bile acids in perfused rat liver subjected to chronic biliary drainage. Biochem. J. 1970; 118:519–530. [PubMed: 5472179]

[7]. Casaschi A, Maiyoh GK, Rubio BK, Li RW, et al. The chalcone xanthohumol inhibits triglyceride and apolipoprotein B secretion in HepG2 cells. J. Nutr. 2004; 134:1340–1346. [PubMed: 15173394]

[8]. Nozawa H. Xanthohumol, the chalcone from beer hops (*Humulus lupulus* L.), is the ligand for farnesoid X receptor and ameliorates lipid and glucose metabolism in KK-A(y) mice. Biochem. Biophys. Res. Commun. 2005; 336:754–761. [PubMed: 16140264]

[9]. Yang JY, Della-Fera MA, Rayalam S, Baile CA. Effect of xanthohumol and isoxanthohumol on 3T3-L1 cell apoptosis and adipogenesis. Apoptosis. 2007; 12:1953–1963. [PubMed: 17874298]

[10]. Legette LL, Moreno Luna AY, Reed RL, Miranda CL, et al. Xanthohumol lowers body weight and fasting plasma glucose in obese male Zucker fa/fa rats. Phytochemistry. 2012 DOI: 10.1016/j.phytochem.2012.04.018.

[11]. Cho YC, Kim HJ, Kim YJ, Lee KY, et al. Differential anti-inflammatory pathway by xanthohumol in IFN-gamma and LPS-activated macrophages. Int. Immunopharmacol. 2008; 8:567–573. [PubMed: 18328448]

[12]. Cho YC, You SK, Kim HJ, Cho CW, et al. Xanthohumol inhibits IL-12 production and reduces chronic allergic contact dermatitis. Int. Immunopharmacol. 2010; 10:556–561. [PubMed: 20144742]

[13]. Lupinacci E, Meijerink J, Vincken JP, Gabriele B, et al. Xanthohumol from hop (*Humulus lupulus* L.) is an efficient inhibitor of monocyte chemoattractant protein-1 and tumor necrosis factor-alpha release in LPS-stimulated RAW 264.7 mouse macrophages and U937 human monocytes. J. Agric. Food Chem. 2009; 57:7274–7281. [PubMed: 19634869]

[14]. Plump AS, Smith JD, Hayek T, Aalto-Setala K, et al. Severe hypercholesterolemia and atherosclerosis in apolipoprotein E-deficient mice created by homologous recombination in ES cells. Cell. 1992; 71:343–353. [PubMed: 1423598]

[15]. Chandak PG, Obrowsky S, Radovic B, Doddapattar P, et al. Lack of acyl-CoA:diacylglycerol acyltransferase 1 reduces intestinal cholesterol absorption and attenuates atherosclerosis in apolipoprotein E knockout mice. Biochim. Biophys. Acta. 2011; 1811:1011–1020. [PubMed: 21924378]

[16]. Wakil SJ, Stoops JK, Joshi VC. Fatty acid synthesis and its regulation. Annu. Rev. Biochem. 1983; 52:537–579. [PubMed: 6137188]

[17]. Munday MR, Campbell DG, Carling D, Hardie DG. Identification by amino acid sequencing of three major regulatory phosphorylation sites on rat acetyl-CoA carboxylase. Eur. J. Biochem. 1988; 175:331–338. [PubMed: 2900138]

[18]. Witters LA, Nordlund AC, Marshall L. Regulation of intracellular acetyl-CoA carboxylase by ATP depletors mimics the action of the 5′-AMP-activated protein kinase. Biochem. Biophys. Res. Commun. 1991; 181:1486–1492. [PubMed: 1684896]

[19]. Muoio DM, Seefeld K, Witters LA, Coleman RA. AMP-activated kinase reciprocally regulates triacylglycerol synthesis and fatty acid oxidation in liver and muscle: evidence that sn-glycerol-3-phosphate acyltransferase is a novel target. Biochem. J. 1999; 338(Pt 3):783–791. [PubMed: 10051453]

[20]. Winder WW, Hardie DG. AMP-activated protein kinase, a metabolic master switch: possible roles in type 2 diabetes. Am. J. Physiol. 1999; 277:E1–E10. [PubMed: 10409121]

[21]. Legette L, Ma L, Reed RL, Miranda CL, et al. Pharmacokinetics of xanthohumol and metabolites in rats after oral and intravenous administration. Mol. Nutr. Food Res. 2012; 56:466–474. [PubMed: 22147307]

[22]. Hanske L, Loh G, Sczesny S, Blaut M, et al. Recovery and metabolism of xanthohumol in germ-free and human microbiota-associated rats. Mol. Nutr. Food Res. 2010; 54:1405–1413. [PubMed: 20397197]

[23]. Boring L, Gosling J, Cleary M, Charo IF. Decreased lesion formation in CCR2−/− mice reveals a role for chemokines in the initiation of atherosclerosis. Nature. 1998; 394:894–897. [PubMed: 9732872]

[24]. Gosling J, Slaymaker S, Gu L, Tseng S, et al. MCP-1 deficiency reduces susceptibility to atherosclerosis in mice that overexpress human apolipoprotein B. J. Clin. Invest. 1999; 103:773–778. [PubMed: 10079097]

[25]. Hirata H, Yimin, Segawa S, Ozaki M, et al. Xanthohumol prevents atherosclerosis by reducing arterial cholesterol content via CETP and apolipoprotein E in CETP-transgenic mice. PLoS One. 2012; 7:8.

[26]. Dorn C, Massinger S, Wuzik A, Heilmann J, et al. Xanthohumol suppresses inflammatory response to warm ischemia-reperfusion induced liver injury. Exp. Mol. Pathol. 2012; 94:10–16. [PubMed: 22634733]

[27]. Monteiro R, Calhau C, Silva AO, Pinheiro-Silva S, et al. Xanthohumol inhibits inflammatory factor production and angiogenesis in breast cancer xenografts. J. Cell. Biochem. 2008; 104:1699–1707. [PubMed: 18348194]

[28]. Gao X, Deeb D, Liu Y, Gautam S, et al. Immunomodulatory activity of xanthohumol: inhibition of T cell proliferation, cell-mediated cytotoxicity and Th1 cytokine production through suppression of NF-kappaB. Immunopharmacol. Immunotoxicol. 2009; 31:477–484. [PubMed: 19555200]

[29]. Decleves AE, Mathew AV, Cunard R, Sharma K. AMPK mediates the initiation of kidney disease induced by a high-fat diet. J. Am. Soc. Nephrol. 2011; 22:1846–1855. [PubMed: 21921143]

[30]. Miyokawa-Gorin K, Takahashi K, Handa K, Kitahara A, et al. Induction of mitochondrial uncoupling enhances VEGF(1)(2)(0) but reduces MCP-1 release in mature 3T3-L1 adipocytes: possible regulatory mechanism through endogenous ER stress and AMPK-related pathways. Biochem. Biophys. Res. Commun. 2012; 419:200–205. [PubMed: 22330806]

[31]. Jeong HW, Hsu KC, Lee JW, Ham M, et al. Berberine suppresses proinflammatory responses through AMPK activation in macrophages. Am. J. Physiol. Endocrinol. Metab. 2009; 296:E955–E964. [PubMed: 19208854]

[32]. Ewart MA, Kohlhaas CF, Salt IP. Inhibition of tumor necrosis factor alpha-stimulated monocyte adhesion to human aortic endothelial cells by AMP-activated protein kinase. Arterioscler. Thromb. Vasc. Biol. 2008; 28:2255–2257. [PubMed: 18802013]

[33]. Li Y, Xu S, Mihaylova MM, Zheng B, et al. AMPK phosphorylates and inhibits SREBP activity to attenuate hepatic steatosis and atherosclerosis in diet-induced insulin-resistant mice. Cell Metab. 2011; 13:376–388. [PubMed: 21459323]

[34]. Mao J, DeMayo FJ, Li H, Abu-Elheiga L, et al. Liver-specific deletion of acetyl-CoA carboxylase 1 reduces hepatic triglyceride accumulation without affecting glucose homeostasis. Proc. Natl. Acad. Sci. USA. 2006; 103:8552–8557. [PubMed: 16717184]

[35]. Browning JD, Horton JD. Molecular mediators of hepatic steatosis and liver injury. J. Clin. Invest. 2004; 114:147–152. [PubMed: 15254578]

[36]. Avula B, Ganzera M, Warnick JE, Feltenstein MW, et al. High-performance liquid chromatographic determination of xanthohumol in rat plasma, urine, and fecal samples. J. Chromatogr. Sci. 2004; 42:378–382. [PubMed: 15355578]

[37]. Vanhoecke BW, Delporte F, Van Braeckel E, Heyerick A, et al. A safety study of oral tangeretin and xanthohumol administration to laboratory mice. In Vivo. 2005; 19:103–107. [PubMed: 15796161]

[38]. Hussong R, Frank N, Knauft J, Ittrich C, et al. A safety study of oral xanthohumol administration and its influence on fertility in Sprague Dawley rats. Mol. Nutr. Food Res. 2005; 49:861–867. [PubMed: 16092070]

[39]. Dorn C, Bataille F, Gaebele E, Heilmann J, et al. Xanthohumol feeding does not impair organ function and homoeostasis in mice. Food Chem. Toxicol. 2010; 48:1890–1897. [PubMed: 20427021]

[40]. Sato R, Goldstein JL, Brown MS. Replacement of serine-871 of hamster 3-hydroxy-3-methylglutaryl-CoA reductase prevents phosphorylation by AMP-activated kinase and blocks inhibition of sterol synthesis induced by ATP depletion. Proc. Natl. Acad. Sci USA. 1993; 90:9261–9265. [PubMed: 8415689]

[41]. Clarke PR, Hardie DG. Regulation of HMG-CoA reductase: identification of the site phosphorylated by the AMP-activated protein kinase in vitro and in intact rat liver. EMBO J. 1990; 9:2439–2446. [PubMed: 2369897]

[42]. Namkoong C, Kim MS, Jang PG, Han SM, et al. Enhanced hypothalamic AMP-activated protein kinase activity contributes to hyperphagia in diabetic rats. Diabetes. 2005; 54:63–68. [PubMed: 15616011]

[43]. Albini A, Dell'Eva R, Vene R, Ferrari N, et al. Mechanisms of the antiangiogenic activity by the hop flavonoid xanthohumol: NF-kappaB and Akt as targets. FASEB J. 2006; 20:527–529. [PubMed: 16403733]

[44]. Dell'Eva R, Ambrosini C, Vannini N, Piaggio G, et al. AKT/NF-kappaB inhibitor xanthohumol targets cell growth and angiogenesis in hematologic malignancies. Cancer. 2007; 110:2007–2011. [PubMed: 17823911]

[45]. Yang JY, Della-Fera MA, Rayalam S, Baile CA. Enhanced effects of xanthohumol plus honokiol on apoptosis in 3T3-L1 adipocytes. Obesity (Silver Spring). 2008; 16:1232–1238. [PubMed: 18369342]

[46]. Deeb D, Gao X, Jiang H, Arbab AS, et al. Growth inhibitory and apoptosis-inducing effects of xanthohumol, a prenylated chalone present in hops, in human prostate cancer cells. Anticancer Res. 2010; 30:3333–3339. [PubMed: 20944105]

[47]. Hahn-Windgassen A, Nogueira V, Chen CC, Skeen JE, et al. Akt activates the mammalian target of rapamycin by regulating cellular ATP level and AMPK activity. J. Biol. Chem. 2005; 280:32081–32089. [PubMed: 16027121]

[48]. Hoekstra M, Kruijt JK, Van Eck M, Van Berkel TJ. Specific gene expression of ATP-binding cassette transporters and nuclear hormone receptors in rat liver parenchymal, endothelial, and Kupffer cells. J. Biol. Chem. 2003; 278:25448–25453. [PubMed: 12704191]

[49]. Kennedy MA, Barrera GC, Nakamura K, Baldan A, et al. ABCG1 has a critical role in mediating cholesterol efflux to HDL and preventing cellular lipid accumulation. Cell Metab. 2005; 1:121–131. [PubMed: 16054053]

[50]. Ji A, Wroblewski JM, Cai L, de Beer MC, et al. Nascent HDL formation in hepatocytes and role of ABCA1, ABCG1, and SR-BI. J. Lipid Res. 2012; 53:446–455. [PubMed: 22190590]

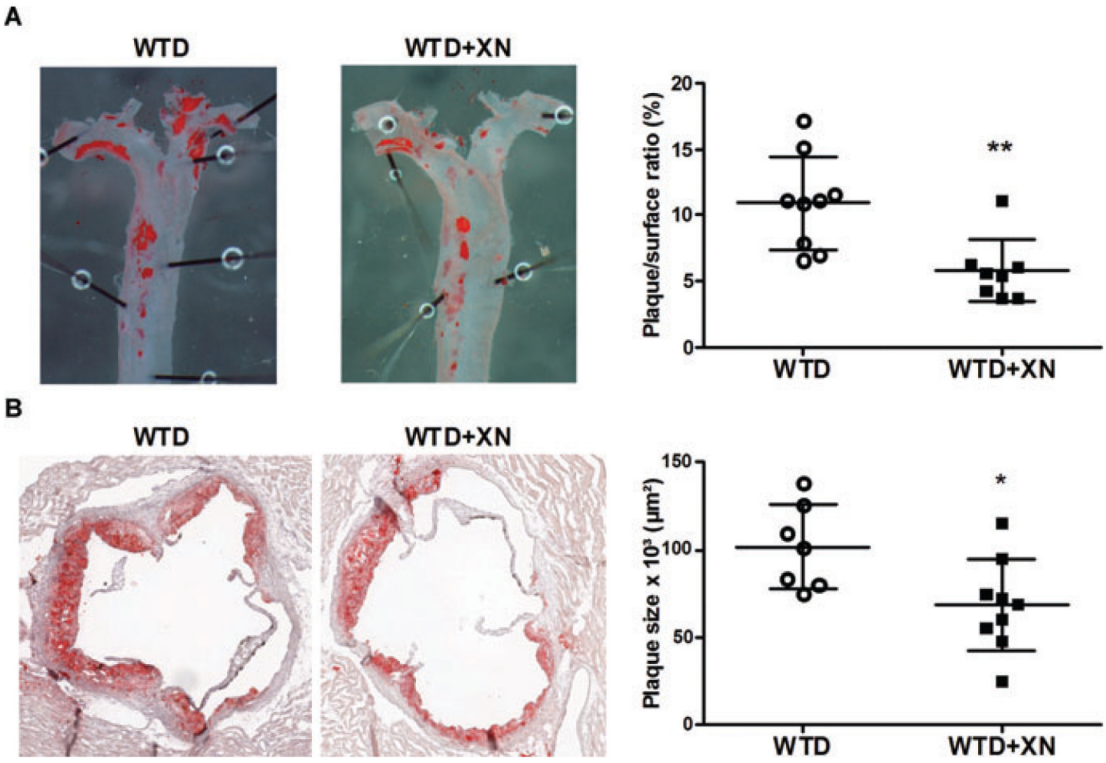

Figure 1.

Reduced plaque formation in XN-fed *ApoE*$^{-/-}$ mice. Female *ApoE*$^{-/-}$ mice were fed WTD ± XN for 8 weeks. (A) Representative images of the descending thoracic aorta. The graph represents mean lesion area relative to the total surface area. $^{**}p \leq 0.01$. (B) Representative images of aortic valve sections. The graph represents mean plaque area calculated from five consecutive sections per mouse. Bars represent the mean values of eight to nine animals ±SD. $^{*}p < 0.05$.

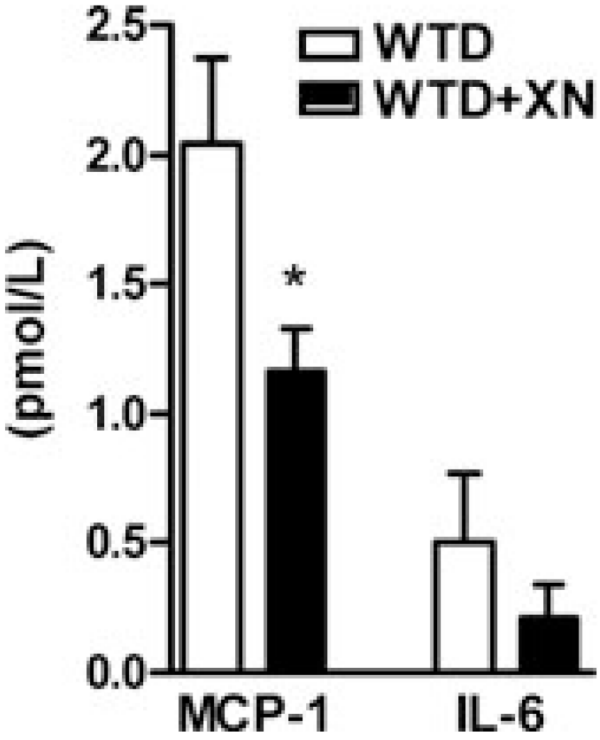

Figure 2.
Reduced MCP-1 concentrations in XN-fed *ApoE*$^{-/-}$ mice. Female *ApoE*$^{-/-}$ mice were fed WTD ± XN for 8 weeks. MCP-1 and IL-6 serum concentrations were determined by ELISA. Data represent mean values ($n = 5$) ± SD. *$p < 0.05$.

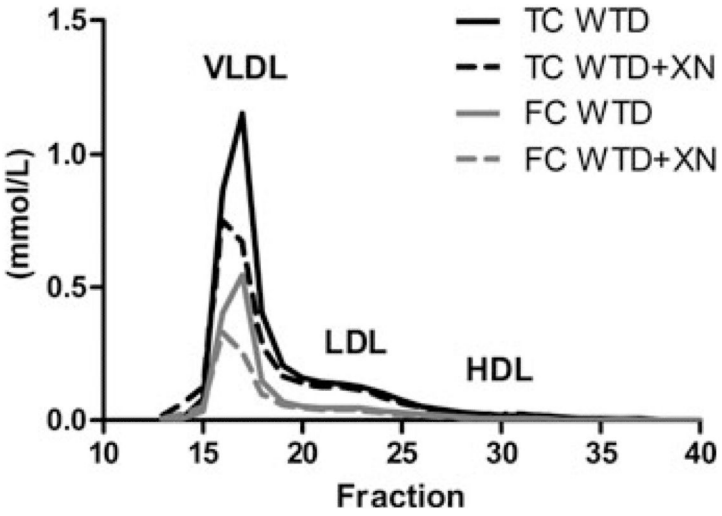

Figure 3.
Decreased cholesterol concentrations in VLDL fraction of XN-fed *ApoE*$^{-/-}$ mice. Lipoprotein profile of pooled plasma samples from overnight fasted *ApoE*$^{-/-}$ mice ($n = 5$) fed WTD ± XN. Total cholesterol (TC) and free cholesterol (FC) concentrations in each fraction after fast protein LC separation were measured enzymatically.

Europe PMC Funders Author Manuscripts

Europe PMC Funders Author Manuscripts

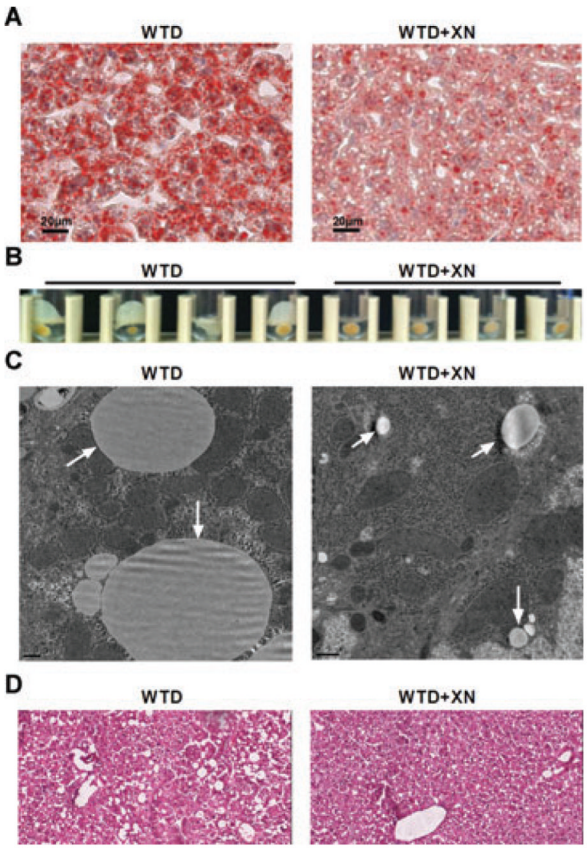

Figure 4.

Reduced lipid content in livers of XN-fed *ApoE*$^{-/-}$ mice. Female *ApoE*$^{-/-}$ mice were fed WTD ± XN for 8 weeks. (A) Representative images of oil red O-stained liver sections. (B) Fat layers after separation of lipids from water soluble components by ultracentrifugation at 100 000 × *g* for 60 min at 4°C. (C) Representative electron microscopy images showing lipid droplets in hepatocytes indicated by white arrows. (D) Representative images of hematoxylin/eosin staining.

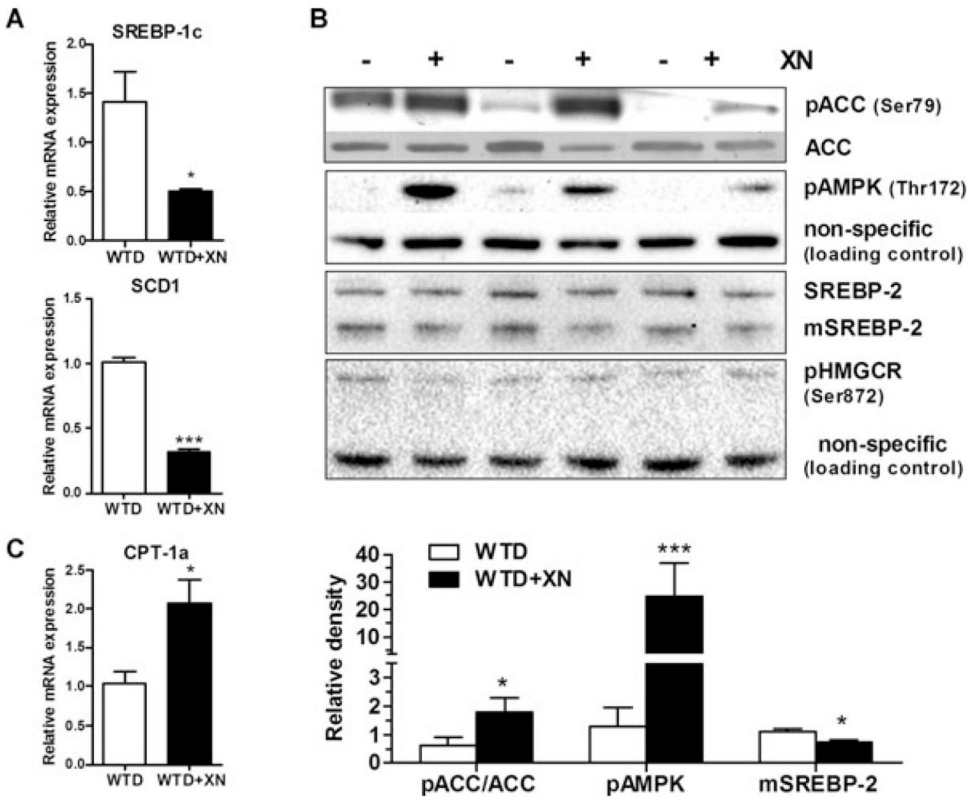

Figure 5.

XN treatment inhibits hepatic lipogenesis and induces fatty acid oxidation in *ApoE*$^{-/-}$ mice. Female *ApoE*$^{-/-}$ mice were fed WTD ± XN for 8 weeks. Livers were excised and protein as well as total RNA were isolated. (A) Quantitative realtime PCR analyses of SREBP-1c, SCD1, and (C) CPT-1a normalized to cyclophilin A. Data are expressed as mean values (n = 4) ± SD. *$p < 0.05$, ***$p \leq 0.001$. (B) Western blotting analyses of proteins involved in fatty acid and cholesterol biosynthesis. Band intensities were quantitated using Image J software. Data represent the ratios of pACC/ACC, pAMPK/loading control, and mSREBP2/SREBP2 from three samples per group ± SD. *$p < 0.05$, ***$p \leq 0.001$.

Europe PMC Funders Author Manuscripts

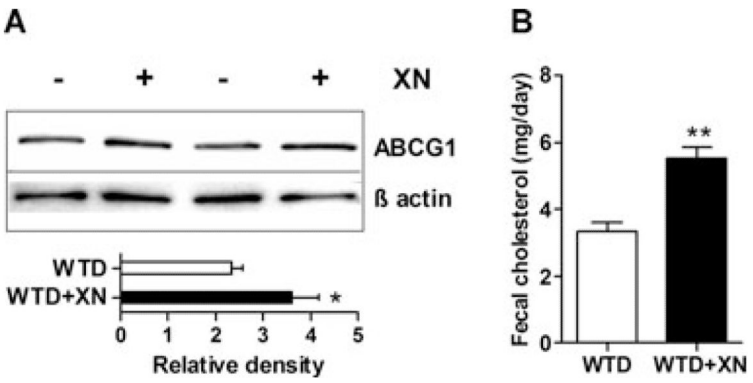

Figure 6.

XN treatment enhances fecal cholesterol excretion in *ApoE*$^{-/-}$ mice fed WTD. Female *ApoE*$^{-/-}$ mice were fed WTD ± XN for 8 weeks. (A) Representative Western blot analysis of ABCG1 from liver lysates of two untreated (−) and two XN-treated (+) mice. The bar graph represents quantifications from samples of $n = 4 \pm$ SD. *$p < 0.05$. (B) Fecal cholesterol levels calculated as mean concentrations ($n = 5$) ± SD of feces collected for three consecutive days. **$p \leq 0.01$.

Europe PMC Funders Author Manuscripts

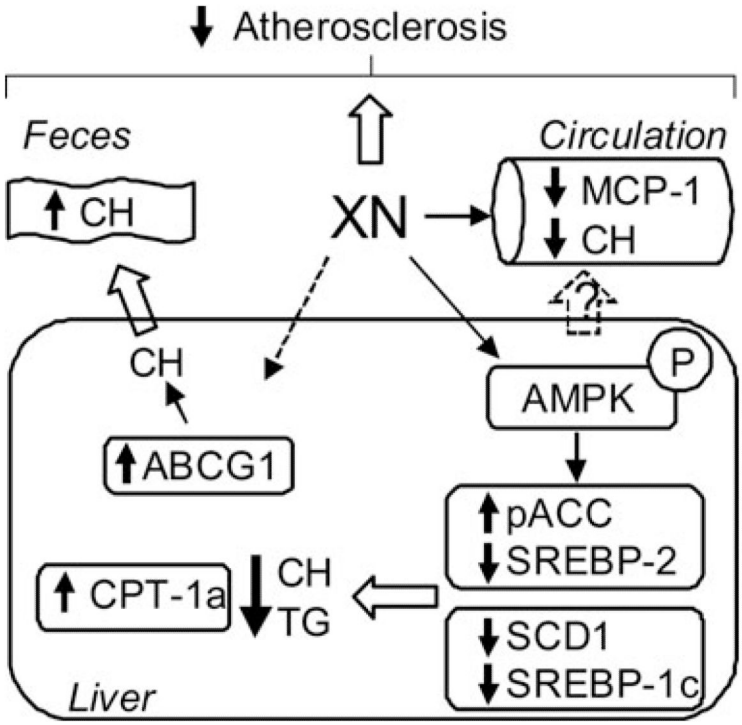

Figure 7.

Schematic summary of the effects of XN feeding to *ApoE*$^{-/-}$ mice. XN administration leads to phosphorylation of hepatic AMPK, which phosphorylates and inactivates ACC, reduces mature SREBP-2 protein and decreases mRNA expression of SREBP-1c and SCD1. In addition, increased expression of CPT-1a suggests increased fatty acid beta-oxidation. As a consequence, de novo lipogenesis in the liver is reduced and fecal cholesterol content is increased. In combination with reduced cholesterol and MCP-1 concentrations in the circulation, XN attenuates atherosclerotic plaque formation in WTD-fed *ApoE*$^{-/-}$ mice. ABC, ATP-binding cassette transporter; ACC, acetyl-CoA carboxylase; AMPK, AMP-activated protein kinase; CH, cholesterol; CPT, carnitine palmitoyltransferase; MCP-1, monocyte chemoattractant protein 1; SREBP, sterol regulatory element-binding protein; TGs, triglycerides; XN, xanthohumol.

Europe PMC Funders Author Manuscripts

Europe PMC Funders Author Manuscripts

Table 1

Reduced plasma cholesterol concentrations in XN-fed *ApoE*$^{-/-}$ mice

	4 weeks		8 weeks	
	WTD (*n* = 10)	**WTD + XN (*n* = 13)**	**WTD (*n* = 8)**	**WTD + XN (*n* = 9)**
TC (mmol/L)	23.8 ± 1	16.3 ± 1***	26.5 ± 0.8	20.3 ± 1.1***
FC (mmol/L)	7.4 ± 0.4	5.4 ± 0.4**	8.3 ± 0.3	6.5 ± 0.4**
CE (mmol/L)	16.2 ± 0.8	10.9 ± 0.6***	18.2 ± 0.6	13.8 ± 0.7***
TG (mmol/L)	0.8 ± 0.1	0.8 ± 0.1	1.2 ± 0.1	1.5 ± 0.2
XN plasma concentrations				
	Fasted plasma		Fed plasma	
XN (nmol/L)	n.d.		61	

ApoE$^{-/-}$ mice were fed WTD ± XN for 8 weeks. Plasma was isolated from overnight fasted mice after 4 and 8 weeks, respectively, and TG, TC, and FC concentrations were measured enzymatically. CE concentrations were calculated as CE = TC − FC.

XN plasma concentrations were measured in pooled samples from WTD + XN-fed *ApoE*$^{-/-}$ mice ($n = 4$) after 4 weeks of feeding.

Data are expressed as mean values ±SD.

n.d., not detected.

** $p \leq 0.01$

*** $p \leq 0.001$.

Europe PMC Funders Author Manuscripts

Table 2

Reduced liver lipid concentrations in XN-fed *ApoE*$^{-/-}$ mice

	WTD (*n* = 9)	WTD + XN (*n* = 9)
TC (mg/g)	7.1 ± 0.5	4.3 ± 0.1 ***
FC (mg/g)	4.2 ± 0.4	2.7 ± 0.2 **
CE (mg/g)	3.6 ± 0.5	1.6 ± 0.2 ***
TG (mg/g)	12 ± 1.1	8.8 ± 0.7 *

Liver lipids (fed state) from *ApoE*$^{-/-}$ mice fed 8 weeks WTD or WTD + XN were extracted by Folch extraction and TG, TC, and FC concentrations were measured enzymatically. CE levels were calculated as CE = TC − FC.

Data represent mean values (*n* = 9) ±SD normalized to wet tissue weight.

* $p < 0.05$

** $p \leq 0.01$

*** $p \leq 0.001$.